Knockout of rbm24a and rbm24b genes in zebrafish impairs skeletal and cardiac muscle integrity and function during development

Audrey Saquet, Ziwei Ying, De-li Shi, Raphaëlle Grifone

Developmental Dynamics / Patterns and Phenotypes

Knockout of *rbm24a* and *rbm24b* genes in zebrafish impairs skeletal and cardiac muscle integrity and function during development

Audrey Saquet[1#], Ziwei Ying[1#], De-Li Shi[1,2*] and Raphaëlle Grifone[1*]

[1]Laboratory of Developmental Biology (LBD), CNRS UMR7622, Institut de Biologie Paris-Seine (IBPS), Sorbonne Université, 75005 Paris, France.
[2]Department of Medical Research, Affiliated Hospital of Guangdong Medical University, Zhanjiang 524001, China.

[#]These authors contributed equally to this work.

*Correspondance to:
Raphaëlle Grifone, Laboratory of Developmental Biology (LBD), CNRS UMR7622, Institut de Biologie Paris-Seine (IBPS), Sorbonne Université, 75005 Paris, France. Adress: 9, Quai Saint-Bernard, case 24, 75005 Paris. E-mail: raphaelle.grifone@sorbonne-universite.fr
De-Li Shi, Laboratory of Developmental Biology (LBD), CNRS UMR7622, Institut de Biologie Paris-Seine (IBPS), Sorbonne Université, 75005 Paris, France. Adress: 9, Quai Saint-Bernard, case 24, 75005 Paris. E-mail: de-li.shi@upmc.fr

Abstract

Backgound: Skeletal and cardiac muscles are contractile tissues whose development and function are dependent on genetic programs that must be precisely orchestrated in time and space. In addition to transcription factors, RNA-binding proteins tightly regulate gene expression by controlling the fate of RNA transcripts, thus specific proteins levels within the cell. Rbm24 has been identified as a key player of myogenesis and cardiomyogenesis in several vertebrates, by controlling various aspects of post-transcriptional regulation, including pre-mRNA alternative splicing and mRNA stabilization. In zebrafish, knockdown of *rbm24a* or *rbm24b* also causes skeletal and cardiac muscle phenotypes, but how their combined loss affects muscle integrity and function remains elusive. **Results:** By genome editing, we have generated *rbm24a* and *rbm24b* single mutants as well as double mutants. Structural analyses indicate that homozygous *rbm24a* and *rbm24b* double mutants exhibit severe somitic muscle and cardiac phenotypes, although *rbm24b* single mutants are obviously normal. We further show that loss of *rbm24a* and *rbm24b* disrupts sarcomere organization, impairing functional contractility and motility of skeletal and cardiac muscles. **Conclusion:** The *rbm24* mutant zebrafish represents a new genetic tool for in-depth studies of Rbm24-mediated post-transcriptional regulation of skeletal and cardiac muscle development, disease and regeneration.

Key words: Rbm24, RNA-binding protein, post-transcriptional regulation, skeletal muscle, heart, sarcomere, zebrafish.

Introduction

RNA-binding proteins (RBPs) are critical regulators of gene expression in a wide variety of cell types from embryogenesis to adulthood. Vertebrate cells encode thousands of RBPs that control various aspects of transcript fates including pre-mRNA alternative splicing, and mRNA stability, transport, subcellular localization, polyadenylation and translation efficiency.[1] RBPs thus serve as critical rheostats of protein accumulation to finely regulate cell proliferation or differentiation in many organs during development, morphogenesis, maturation, function, homeostasis and regeneration.[1] Due to their crucial role in gene expression, it is not surprising that dysregulation of RBPs can compromise cellular health and function. Accordingly, numerous monogenic diseases in humans are caused by damaging mutations in RBP genes or by indirect RBP protein dysfunctions.[2]

Skeletal and cardiac muscles are contractile tissues whose development, homeostasis and function require specific post-transcriptional networks that are regulated by a large repertoire of RBPs. The functional cellular unit of all skeletal muscles, the multinucleated myofibers, is formed by the proliferation, differentiation and fusion of mononucleated myoblasts, which are largely controlled by various RBPs in parallel to different transcription factors.[3] The maturation of such muscle cells, with the appearance of contractile proteins and their organization into myofilaments and myofibrils, is also strongly regulated at the post-transcriptional level during embryogenesis. In adult muscles, RBPs contribute to the maintenance of tissue homeostasis and the process of regeneration, often in a similar manner as they function in the embryonic myogenic cells. The heart, as the first organ forming during embryonic development and the first acquiring functionality, derives from the establishment of specific cardiac cell types and the development of a primitive heart tube, followed by morphogenesis, remodeling, and postnatal maturation. In addition to transcriptional regulation, these steps are also orchestrated by post-transcriptional networks involving hundreds of RBPs, some of which display shared functions in skeletal muscle development.[4-6]

This is particularly the case for the RNA binding motif protein Rbm24, which harbors an N-terminal RNA recognition motif (RRM) and is expressed in several tissues of vertebrate embryos, including embryonic and adult skeletal and cardiac muscles.[7-12] Several studies have demonstrated that Rbm24 is a key player of skeletal muscle cell specification, differentiation and regeneration in vertebrates, by functioning in multiple

aspects of post-transcriptional regulation, including pre-mRNA alternative splicing and mRNA stabilization.[13-17] We have reported that in chick embryos and in adult mice, knockdown of *Rbm24* in myogenic progenitors severely disrupts their differentiation likely due to impaired expression and defective pre-mRNA alternative splicing of muscle-specific genes.[8,11] Rbm24 has also been highlighted as a pivotal regulator of cardiomyocyte patterning and cardiac sarcomerogenesis during different stages of heart morphogenesis primarily by functioning as a splicing factor.[14,16,17] In addition, conditional knockout of *Rbm24* in mice suggests that it is required for postnatal cardiac tissue homeostasis.[14] During heart development, Rbm24 not only regulates splicing but also controls the translation of its mRNA targets, as demonstrated in the mouse embryo.[18] Indeed, through interaction with the eukaryotic initiation factor 4E (eIF4E) to prevent its association with the 5'-cap of *p53* mRNA and the formation of translation initiation complex, Rbm24 act as a repressor of *p53* mRNA translation in cardiac cells, thus protecting heart development via reduced cell cycle arrest and/or apoptosis.[18]

Studies in zebrafish have pointed a conserved role of Rbm24 in cardiac development. There are two *rbm24* paralogs in zebrafish, *rbm24a* and *rbm24b*, due to duplication of the major part of the genome. It has been shown that morpholino-mediated knockdown of *rbm24a* or *rbm24b* causes heart developmental defects.[10,19] By genome editing, we have generated a zebrafish *rbm24a* mutant line and found that loss of *rbm24a* produces similar heart defects.[20] These studies suggest a critical role of *rbm24a* in heart development. However, it remains unclear how combined loss of *rbm24a* and *rbm24b* affects skeletal muscle formation and myocardial organization. In the present study, we generated *rbm24a* and *rbm24b* double homozygous mutants to characterize skeletal and cardiac muscle phenotypes. While *rbm24a* single mutants display weak skeletal muscle defects and strong cardiac abnormalities, *rbm24b* single mutants show no obvious phenotype. However, simultaneous loss of *rbm24a* and *rbm24b* most severely disrupts muscle tissue integrity and function. These results further confirm the muscle regulatory role of Rbm24 in different vertebrates,[8,21,22] and uncover a functional redundancy of zebrafish *rbm24a* and *rbm24b* in striated muscle development. Our study thus provides a new genetic tool to assess for the function of Rbm24 in skeletal and cardiac muscle development and function in vertebrates.

Results

Zebrafish *rbm24a* and *rbm24b* are expressed in restricted regions during embryogenesis

Zebrafish genome harbors *rbm24a* and *rbm24b*. Their expression has been previously reported for several developmental stages.[10,19,22] However, the onset of *rbm24a* and *rbm24b* expression in somitic mesoderm and cardiac precursors has not been clearly determined. In order to extend the analysis, we performed whole-mount in situ hybridization (WISH) experiments to monitor the detailed expression patterns of *rbm24a* and *rbm24b* across 16 time points, from 8-somite stage (between 12 and 14 hpf) to 31 hpf.

The expression of *rbm24a* was first evident in the developing somites at least at 8-somite stage (Figure 1A). At 14 hpf when the embryo has formed 10 somites, *rbm24a* expression was present in segmented somites at the anterior region, with the transcripts detected in laterally located slow muscle cells and in medially located fast muscle cells (Figure 1B,Q,Q'); in the posterior region, *rbm24a* transcprits were solely detected in the most medial part of the unsegmented paraxial mesoderm, which corresponds to the progenitors of the slow twitch muscle lineage, namely adaxial cells, known to further migrate laterally (Figure 1B,R,R'). A similar expression pattern could be observed from 12- to 20-somite stages (Figure C-F). From 22-somite stage to the end of the segmentation period at 24 hpf, *rbm24a* expression was detected in all differentiated muscle cells within the somites, including medially located fast muscles and laterally located slow muscles (Figure 1G-J,S-S'''), as well was in the most caudal somites (Figure 1K,T-T''). As development proceeds, *rbm24a* expression gradually declined in the anterior region to become restricted to the most caudal somites (Figure 1I-P). Therefore, *rbm24a* shows strong expression in both slow and fast muscle cells, which are originated from the segmental plate.[27]

We also monitored *rbm24a* expression in the developing heart. Its transcripts were not detected in the presumptive heart region at 8-somite stage but were present in the heart primordium at 10-somite stage (Figure 1A,B). From 10- to 18-somite stages, *rbm24a* expression was detected in the bilateral cardiac fields (Figure 1B-E,U-W), which normally are composed of differentiated ventricular myocytes closest to the midline and undifferentiated atrial precursors located laterally.[28] From 22- to 24-somite stages, the bilateral myocardial heart fields have migrated toward the midline and fused to form a

disc structure expressing *rbm24a* (Figure 1G,H,X). The expression of *rbm24a* was maintained in the developing heart from 22 hpf until at least 31 hpf (Figure 1I-P). Therefore, our results clearly show that *rbm24a* expression is initiated in the bilateral heart fields at least at 14 hpf when the embryo has formed 10 somites. In addition to the skeletal and cardiac muscle territories, *rbm24a* was also detected in the developing ear and eye. It was detected in the otic vesicle from 12-somite stage onward (Figure 1C-P,U-X) and was expressed in the developing lens from 18-somite stage onward (Figure 1E-P).

We also examined the expression of *rbm24b* during early development from 12-somite stage to 24 hpf. The results indicated that *rbm24b* expression was only present in the developing somites. At all stages examined, it was detected in both segmented somites and unsegmented presomitic mesoderm, including medially located fast muscle precurdors and laterally located slow muscle precursors (Figure 2A-M). Thus, compared with *rbm24a*, *rbm24b* was expressed in the entire paraxial mesoderm from 10-somite stage to at least 24 hpf, whereas *rbm24a* expression is progressively restricted to posterior somitic mesoderm. Despite intense staining present in the somites, we did not detect obvious *rbm24b* expression in the developing heart (Figure 2A-J). However, by increasing the incubation period for chromogenic reaction, weak staining could be observed in the heart area at 24 hpf similarly to published results (Figure 2K). Thus, it is possible that *rbm24b* displays very weak expression in the heart.

Phenotype analyses of zebrafish *rbm24a* and *rbm24b* double homozygous mutants

Rbm24a and Rbm24b proteins exhibit high level of overall identity, particularly in the RRM located at the N-terminal half. This suggests that they may display redundant functions in the post-transcriptional regulation of gene expression. We have previously generated an *rbm24a* mutant line.[20] To investigate the functional role of *rbm24a* and *rbm24b* in zebrafish embryonic development, we used the CRISPR/Cas9 system to produce mutation in the *rbm24b* locus. An indel (-8/+15 base pairs) was created in the first exon. This mutation is predicated to cause frameshift at the beginning of the coding region, thus disrupting the expression of Rbm24b protein (Figure 3). Phenotype analysis indicated that homozygous *rbm24b* mutants developed normally without obvious phenotype (Figure 4).

Since homozygous *rbm24a* mutants are embryonically lethal, we first generated triallelic *rbm24a*$^{+/-}$;*rbm24b*$^{-/-}$ mutants that are heterozygous for *rbm24a* and homologous for *rbm24b*. Double homozygous *rbm24a* and *rbm24b* (*rbm24a*$^{-/-}$;*rbm24b*$^{-/-}$) mutant embryos can be obtained by crossing these triallelic carriers. The phenotype of *rbm24a*$^{-/-}$;*rbm24b*$^{-/-}$ mutants was examined from 1.5 dpf to 5 dpf (Figure 5). Double homozygous *rbm24a* and *rbm24b* mutant embryos first presented a pericardial edema that became apparent at 1.5 dpf and extended progressively to the abdominal region from 2 dpf to 5 dpf. The anteroposterior axis also became progressively shortened, and most double homozygous mutants developed a curved tail presumably due to defects in somitic derivatives. Double homozygous *rbm24a* and *rbm24b* mutant embryos develop these cardiac and muscle phenotypes with 100% penetrance. In addition, compared with *rbm24a* single mutants, it was apparent that the loss of both *rbm24a* and *rbm24b* led to more severe developmental defects at all stages examined. These observations indicate that Rbm24 plays a predominant role in heart development. Thus, the *rbm24a* and *rbm24b* mutants represent an important genetic tool for the study of Rbm24-regulated events during embryonic cardiac differentiation.

Skeletal and cardiac muscle tissue integrity and function are severely affected following simultaneous loss of *rbm24a* and *rbm24b*

Given the overlapping expression pattern of *rbm24a* and *rbm24b* during somitic muscle differentiation, we further examined how their combined loss affects muscle development. After phalloidin staining of actin filaments to visualize all somites, we found that *rbm24a*$^{-/-}$;*rbm24b*$^{-/-}$ mutants exhibited a significantly reduced muscle tissue (Figure 6A-D), with nearly 30% loss when compared to wild-type embryos at all stages examined ($p<0,0001$ at 2 dpf, $p=0,0021$ at 3 dpf, and $p=0,0342$ at 4 dpf). With respect to wild-type embryos, *rbm24a* single mutants showed a similar reduction of the muscle tissue ($p=0,0051$ at 2 dpf, $p=0,0022$ at 3 dpf, and $p=0,0117$ at 4 dpf), but no significant differences were observed when compared with *rbm24a* and *rbm24b* double mutants (Figure 6D). We then performed a more detailed examination of muscle tissue architecture by confocal microscopy analysis. At 2 dpf, myofibers were irregular in *rbm24a* single mutants when compared with wild-type embryos (Figure 6E-E'). However, myofiber organization was more severely affected in *rbm24a*$^{-/-}$;*rbm24b*$^{-/-}$ mutants (Figure 6E"). They appeared thinner, twisted and loosely arranged, forming a less compact tissue. At 3 dpf, muscle defects in double mutants were exacerbated with the appearance of damaged and disrupted myofibers within the muscle masses (Figure

6F-F"). Using transmission electron microscopy (TEM), we further characterized the muscle phenotype at the ultrastructural level. The results revealed that A-band and I-band patterning in *rbm24a*$^{-/-}$*;rbm24b*$^{-/-}$ mutants was severely disrupted by the accumulation of disordered sarcoplasmic reticulum (Figure 6G,G'), thus affecting sarcomere alignment which is critical for myofibril contraction.

To corroborate the requirement of *rbm24a* and *rbm24b* for muscle development, we performed a touch-evoked tactile stimulation response assay, which is reflective of muscle performance and function,[29] using a tracking protocol to allow the assessment of swimming speed in zebrafish larvae.[24] The results clearly revealed a skeletal muscle dysfunction (Figure 6H). At 2 dpf, 3 dpf, and 4 dpf, *rbm24a*$^{-/-}$*;rbm24b*$^{-/-}$ mutant embryos exhibited significantly slower swimming responses compared to controls (p=0,0018 at 2 dpf, p<0,0001 at 3 dpf and p=0,0001 at 4 dpf). This assay also revealed that double mutants displayed more severe muscle contractile defects than *rbm24a* single mutants (p=0,0487 at 2 dpf, p=0,0056 at 3 dpf and p=0,0223 at 4 dpf). (Figure 6H). These observations indicate that the combined loss of *rbm24a* and *rbm24b* more severely affects skeletal muscle integrity and function, which is consistent with the strong expression of both paralogs in the somites.

The disorganization of cardiac muscle in *rbm24a*$^{-/-}$*;rbm24b*$^{-/-}$ mutants was also characterized using confocal microscopy and TEM. We first used the ventricle-specific MF20 antibody and the atrium-specific S46 antibody to examine morphological changes of the two cardiac chambers at 3 dpf and 4 dpf (Figure 7A-B'). In *rbm24a*$^{-/-}$*;rbm24b*$^{-/-}$ mutants, the ventricle appeared shriveled and smaller, while the atria was overtly dilated. Moreover, the atrium was abnormally positioned posteriorly to the ventricle in mutant embryos, suggesting looping defects (Figure 7C-D'). Confocal sections showed that the atrioventricular canal that divides the heart into two chambers was narrower in *rbm24a*$^{-/-}$*;rbm24b*$^{-/-}$ mutant embryos at 3 dpf and 4 dpf, presumably as a result of the shrinking of the ventricle and the enlargement of the pericardium, pulling the atrium away from the ventricle (Figure 7C-D'). By measuring the cross-sectional areas of heart chambers on confocal sections (Figure 7E,F), we found that the ventricular area in *rbm24a*$^{-/-}$*;rbm24b*$^{-/-}$ mutants was significantly reduced (p=0,0001 at 3dpf and p=0,0002 at 4 dpf), whereas the atrium area was significantly expanded (p=0,0033 at 3 dpf and p=0,0021 at 4 dpf). We then examined sarcomere organization in cardiomyocytes by TEM at 3 dpf. Analysis of longitudinal sections of the heart revealed that control embryos displayed intact sarcomeres with clearly defined Z-disks and well-organized

myofibrils (Figure 7G). By contrast, *rbm24a*$^{-/-}$*;rbm24b*$^{-/-}$ mutant embryos showed disorganized and loosely arranged myofibrils. The Z-disks were often disrupted or absent (Figure 7G'). These results indicate that loss of *rbm24a* and *rbm24b* leads to a complete disorganization of myofibrils and destabilization of sarcomeres in cardiac muscles.

We next performed video recording to measure the heart rate by direct counting of ventricle beating, which revealed a disrupted cardiac function (Figure 7H). At different stages, the heart rate in *rbm24a*$^{-/-}$*;rbm24b*$^{-/-}$ mutant embryos was significantly lower than controls. In addition, while the heart rate increased in wild-type embryos as development proceeds, ~~control,~~ it decreased dramatically at 4 dpf in *rbm24a*$^{-/-}$*;rbm24b*$^{-/-}$ mutants (Figure 7H). Since it is not obvious to unequivocally compare myocardium phenotypes between *rbm24a* single mutants and *rbm24a*$^{-/-}$*;rbm24b*$^{-/-}$ double mutants, we recorded heart rate to reflect the extent of cardiac functional defects. The results indicated that cardiac contractile function was more severely affected in double mutants (Figure 7H). Altogether, these data demonstrate that *rbm24a* and *rbm24b* contribute to maintain the structural integrity and, consequently, the function of cardiac muscles during zebrafish development. However, *rbm24a* clearly plays a predominant role.

Compromised locomotion in *rbm24a*$^{-/-}$*;rbm24b*$^{-/-}$ mutants due to impaired fast and slow muscle differentiation but not altered muscle attachment nor absence of neuromuscular junctions

In the somites, fast-twitch fibers form the bulk of the myotome. Slow fibers cover the myotome and are responsible for the earliest side-to-side contractions of the trunk at 17 hpf, inducing spontaneous tail coiling. At more late stages, slow and fast myofiber contractions are both responsible for controlled swimming behavior, such as short burst movements in response of external stimuli.[35] To examine how slow and fast muscle tissue integrity was affected in the absence of *rbm24a* and *rbm24b*, we performed immunofluorescence staining using antibodies against fast and slow muscle heavy chains. In *rbm24a*$^{-/-}$*;rbm24b*$^{-/-}$ mutants, both fast and slow muscles displayed distorted architecture, and myofibers appeared wavy and were separated by large gaps (Figure 8A-D'). This is consistent with the expression of both *rbm24* paralogs in slow and fast muscle precursors. Altogether, these results indicate that the compromised locomotion of *rbm24a*$^{-/-}$*;rbm24b*$^{-/-}$ mutants is specifically caused by a failure of muscle differentiation and maturation into a fully functional tissue, affecting similarly slow and fast muscles.

The myotendinous junction (MTJ) is an integrated mechanical unit located at the interface of muscles and tendons, transducing muscle contraction force to the skeletal system. It is formed by a highly specialized protein complex, consisting of subsarcolemal transmembrane proteins as well as extracellular matrix components, among which laminin proteins connect muscular sarcomeric actin to tendinous extracellular matrix.[30] Mutations in many genes encoding MTJ components cause various forms of congenital muscle dystrophy by disrupting the myotendinous junction.[31,32] In zebrafish, multinucleated myofibers span the entire myotome of each somite up to the vertical myosepta, which are functionally equivalent to the mammalian tendons. Thus, the myosepta, connecting adjacent muscle cells, transmit muscular forces between axial muscles via the MTJ during fish swimming. Functional disruption of several genes expressed during MTJ formation, including for example *Col22a1* and laminin *alpha2*, leads to the disorganization of muscles and an impairment of motility concomitantly to abnormal myosepta and MTJ.[33,34] Given the altered skeletal muscle integrity and function in *rbm24a*$^{-/-}$*;rbm24b*$^{-/-}$ mutants, we further examined the formation of MTJ by immunofluorescence staining of myotendinous junction. Analysis by confocal optical sectioning indicated that myofibers were severely disorganized in *rbm24a*$^{-/-}$*;rbm24b*$^{-/-}$ mutants, however, myotendinous junctions at the somite boundaries exhibited a regular V-shaped pattern, similarly to control embryos, although laminin immunofluorescence staining became relatively weak at 3 dpf (Figure 9A-F”). The altered locomotion displayed by *rbm24a*$^{-/-}$*;rbm24b*$^{-/-}$ mutants prompted us to examine whether neuromuscular junctions (NMJs) could be affected. Analysis of NMJs, by targeting acetylcholine receptors using rhodamine-conjugated alpha-Bungarotoxin reveals that motor synapses are present and that they are arborized in misaligned and sparse myofibers of the mutants in a smilar pattern as those vizualized in the controls (Figure 10A-B’).

Discussion

Skeletal myogenesis and cardiomyogenesis are developmental processes that require an elaborated interplay of transcriptional and post-transcriptional regulators to sequentially control progenitor cell maintenance, lineage specification, cell determination, proliferation, and finally early and terminal differentiation. In addition to transcription factors, the discovery that specific RBPs are crucial regulators of the protein set-up was a landmark in our understanding of the processes leading to muscle and cardiac cell differentiation.[3,5] This is particularly the case for Rbm24 which recently appeared as a key myogenic and cardiomyogenic factor.[3,5]

In the present study, we report that zebrafish *rbm24a* and *rbm24b* genes are necessary for muscle and cardiac cell differentiation into functional tissues during embryogenesis. We show that double homozygous *rbm24a* and *rbm24b* mutants develop a cardiac phenotype and do not survive beyond 6 dpf. The phenotype of shriveled ventricle, dilated atria and impaired cardiac contractility, associated with disrupted sarcomeric structure in cardiomyocytes, clearly indicate that *rbm24a* and *rbm24b* function redundantly and are essential to drive cardiomyocyte differentiation. Importantly, these results recapitulate and complement previously described morphant phenotype.[10,19] Our observations also clearly indicate that Rbm24 play a predominant role in maintain cardiomyocyte integrity and function. In addition, another novel finding made in this study is that double homozygous *rbm24a* and *rbm24b* mutants develop a strong somitic muscle phenotype with obvious structural alterations at cellular and ultrastructural levels, impairing functional contractility and motility. Therefore, these results reinforce the myogenic function demonstrated for Rbm24 in other vertebrates, thus reconciling the fact that its role is conserved during vertebrate evolution.

The key role of *rbm24a* and *rbm24b* during heart and muscle development, which are highly time-coordinated events with multiple steps occurring in a specific sequence, suggest that their spatial and temporal expression must be tightly regulated. We show that *rbm24a* expression is activated from specification to differentiation of muscle cells. Although the cardiac expression of *rbm24b* is particularly weak, its function can be revealed by the exacerbated cardiac edema phenotype and more severely reduced heart rate in double homozygous *rbm24a* and *rbm24b* mutants. Interestingly, we show that *rbm24a* is expressed in bilateral heart fields, suggesting that it may play an early role in the developing heart. It will be of interest to investigate the molecular

mechanisms governing *rbm24a* expression. Nkx2.5, the earliest marker of cardiac progenitor emergence in zebrafish, controls transcriptional activation of the cardiac gene program in cooperation with other key factors such as *Gata5*, *Hand2* and *Tbx5*.[36] This raises a possibility that *rbm24a* may function downstream of those factors during heart development.

We have shown that the loss of *rbm24a* and *rbm24b* causes severe damages in skeletal muscles and in heart tissues. This is associated with severe alteration in myofibrillogenesis, impairing functionality of these tissues. Since myogenesis and cardiomyogenesis does not seem to be affected at early stages, *rbm24a* and *rbm24b* may not be involved in cell specification but is specifically required for the maturation of differentiated myogenic and cardiomyogenic cells. This conclusion is consistent with the implication of Rbm24 in myogenic differentiation during adult skeletal muscle regeneration.[11,38] The major regulatory role demonstrated so far for Rbm24 resides in the control of specific alternative splicing orchestrating sarcomere assembly and integrity. Indeed, the absence of sarcomere in cardiomyocytes and altered myofibrillogenesis in skeletal muscle cells observed in *Rbm24* knockout mice were associated with impaired exon inclusion in several sarcomeric genes.[17] Postnatal cardiac-specific ablation of *Rbm24* in mice leads to dilated cardiomyopathy and affects a large number of splicing switches.[14] Deletion of *RBM24* in human embryonic stem cells disrupts sarcomeric structures associated to defective splicing of core myofibrillogenesis genes such as *ACTININ-2*, *TITIN* and *MYH10*.[39] Although less extensively analyzed, Rbm24 also functions to regulate the stability of *p21*, *p63* and *myogenin* mRNAs by binding to 3'-untranslated regions.[13,40,41] We recently identified a novel role for Rbm24 in controlling cytoplasmic polyadenylation and translation efficiency in the lens.[20] Thus, Rbm24 appears to be a multitasking RBP capable of regulating target mRNAs through different post-transcriptional mechanisms.

In conclusion, we have generated *rbm24a* and *rbm24b* double homozygous mutants in zebrafish, and our study clearly shows that *rbm24a* and *rbm24b* may have redundant functions in myogenesis and cardiomyogenesis by regulating muscle tissue integrity and function. Although no RBM24 mutation has been yet associated to human disease, it cannot be excluded that dysregulated expression or dysfunction of RBM24 may be present in specific cases of cardiomyopathy or muscle dystrophy patients. The *rbm24* mutant zebrafish will be a useful tool for further study of Rbm24-mediated post-transcriptional regulation in muscle development, disease and regeneration.

Experimental Procedures

Ethic statement for zebrafish handling

Zebrafish embryos were maintained in E3 medium (5 mM NaCl, 0.17 mM KCl, 0.33 mM CaCl2, 0.33 mM MgSO4) at 28°C using a temperature-controlled incubator. All experiments were performed in agreement with the European Directive 210/63/EU on the protection of animals used for scientific purposes, and the French application decree ‘‘Décret 2013-118’’. The fish facility has been approved by the French ‘‘Service for animal protection and health’’ with approval number B-75-05-25.

Genome editing of *rbm24a* and *rbm24b* loci

Zebrafish *rbm24a* mutants were obtained using the TALEN (transcription activator-like effector nuclease) genome editing technology.[20] The CRISPR/Cas9 system was used to generate rbm24b mutants, with targeting sequence located in the first exon (5’-GAGGATGCACAGCTCTCAGA-3’). The guide RNA (200 pg) was mixed with Cas9 protein (300 pg) and injected into 1-cell stage embryos. Individual adult fish was screened by sequencing PCR products amplified from tail fin genomic DNA using primers 5’-GTATATCGTCTGTAGGCGTGG-3’ and 5’-CGTATCCTCTGGTTTGCC-3’.

Genotyping

Genotyping was processed using High Resolution Melting Analysis (HRMA) of genomic DNA as previously described.[23] PCR primers were designed to specifically amplify rbm24a and rbm24b mutated regions (rbm24a: 5’-ACCAAGATATTTGTCGGCGG-3’ and 5’-CAGGCTGGAATCCGTCGTAT-3’; rbm24b: 5’-GTATATCGTCTGTAGGCGTGG-3’ and 5’-CGTATCCTCTGGATTTGCC-3’). Real-time PCR using SsoFastTM EvaGreen1 Supermix (Bio-Rad) with 2 to 15 ng genomic DNA and 0.5 µM of each primer in a 20 µL reaction mixture was performed in a CFX96 system (BioRad). Thermal melting profiles were obtained in the same device by increasing temperature from 75 to 95˚C using a temperature increment of 0.2˚C. They were normalized as previously described.[24] In different experiments, embryos were individually genotyped after imaging.

Whole-mount in situ hybridization

DNA template for generating *rbm24a* and *rbm24b* probes were obtained by PCR amplification of embryonic cDNAs (rbm24a: 5’-CCACATACACCAAGATCTTC-3’ and 5’-AATGATCATCCTCGCTGTCT-3’; rbm24b: 5’-CCACATACACCAAGATCTTC-3’ and 5’-

AATGATCATCCTCGCTGTCT-3'). PCR products were cloned in pGEM-T easy vector and antisense probes were synthesized using appropriate RNA polymerases and digoxigenin-11-UTP (Roche Diagnostics). Embryos were fixed in 4% paraformaldehyde at 4°C overnight. In situ hybridization was performed according to published protocol.[25] Embryos after 24 hpf (hours post-fertilization) were treated with proteinase K (10 µg/mL) for 15 min. Vibratome sections of 100 µm were performed from labeled embryos casted in 6 % low melting agarose. Sections were collected in 1x PBS and mounted in aqueous mounting medium. Embryos and sections were imaged using a stereomicroscope (S8 APO, Leica) or a fluorescence microscope (Leica DM 2500).

Phalloidin, alpha-bungarotoxin and DAPI staining

Embryos were fixed in 4% paraformaldehyde at 4°C overnight, washed in PBS and whole-mount stained with rhodamine-labeled phalloidin (Sigma-Aldrich) at 50 µg/mL diluted in PBS. Embryos older than 2 dpf (days post-fertilization) were permeabilized overnight at 4°C using 4% Triton X-100 in PBS prior to incubation in phalloidin or in alpha-bungarotoxin solution. They were extensively washed in PBT (0.1% Tween-20 in PBS), counterstained with DAPI and washed in PBS. After staining, embryos were manually deyolked, mounted in 60% glycerol solution and imaged using or a ZEISS 980 Fast-Airyscan II upright confocal microscope. Frozen sections of 14 µm from whole-mount labeled embryos were cut using a cryostat (Leica) and washed in PBS. They were mounted in fluoromount medium (Invitrogen) and imaged using a fluorescence microscope (Leica DM 2500).

Immunofluorescence

For whole-mount immunodetection, embryos were fixed in 4% paraformaldehyde at 4°C overnight, and extensively washed in PBS. Embryos older than 2 dpf were permeabilized as above. They were blocked for 2 hours using 3% BSA (bovine serum albumin) and 0.1% Triton X-100 blocking solution diluted in PBS and then incubated overnight at 4 °C with primary antibodies diluted in blocking solution (Laminin, Sigma, 1/100; S46, DHSB, 1/100; MF20, DHSB, 1/100). After extensive washes in PBT, embryos were incubated overnight at 4°C with alexa-488 or alexa-596 conjugated anti-rabbit or anti-mouse secondary antibodies diluted in blocking solution (Interchim, 1/400). Embryos immunolabeled for laminin were extensively washed in PBT and processed for phalloidin and DAPI staining. Double S46 and MF20 immunostaining was achieved by performing the single immunodetection in succession prior to DAPI staining. Embryos

were imaged on a S8 APO Leica stereomicroscope and on a Zeiss 980 Fast-Airyscan II upright confocal microscope.

For immunodetection on sections, embryos were fixed in 4% paraformaldehyde at 4°C overnight, extensively washed in PBS, incubated in 30% sucrose solution at 4°C overnight, embedded in tissue-freezing medium (Leica, Germany), and frozen in liquid nitrogen-cooled isopentane. Transverse cryosections of 14 µm were obtained using a microtome cryostat (Leica) and washed in PBS. Immunofluorescence staining was performed using F59 and F310 monoclonal mouse antibodies from DHSB (1/200). Images were acquired using a Zeiss Axioimager apotome microscope.

Transmission electron microscopy (TEM)

Embryos were fixed using a mix of glutaraldehyde (2%) and paraformaldehyde (2%) in cacodylate buffer (0.1 M, pH 7.4) for 90 min at room temperature and stored at 4°C. They were then washed five times with cacodylate buffer, postfixed with 1% osmium tetroxide for 1 h on ice, extensively washed with distilled water, and embedded in 4% agarose to help handling at later steps. Samples were gradually dehydrated in ethanol, and embedded in Agar 100 Epoxy resin. Thin sections of 70 nm were collected onto 200 mesh copper grids, stained with uranyl acetate (2.5%) and lead citrate (2%), and coated with 2 nm carbon using the ACE600 apparatus (Leica microsystems). Observations were realized in scanning transmission electron microscopy mode within a field-emission scanning electron microscope GeminiSEM 500 (Zeiss) operated at 29 kV, in bright-field imaging and high-angular annular dark-field modes with a 15 µm aperture. Scan speed and line integration were adjusted during observation to maintain a constant signal-to-noise ratio.

Heart rate and velocity measurements

Heart beats per minute were counted by direct visualization of ventricle beating under an S8 APO Leica stereomicroscope. Room temperature remained constant at 22°C throughout the experiment. Velocity measurements were performed by video-recording the swimming behavior of larvae in response to a tactile stimulation. Embryos were placed individually in a petri dish containing E3 medium on an illuminated stage and tapped on the back of the head with a fine glass pipette tip. Videos were recorded at 25 frames per second. Fiji ImageJ was used to quantify the data, with files imported into ImageJ as FFmpeg movies and thresholding applied to allow visualization of the zebrafish, followed by conversion to a binary image. The trackmate plugin was then

utilized to measure the movement, with manual editing of each reading performed to ensure that the larva is tracked correctly through each video frame.[26] Values for speed were obtained for each embryo. A total of 15 to 20 embryos were analyzed at each condition. Average heart rates and velocity with standard error were plotted and significant deviation was determined in GraphPad Prism using the student's t-test.

Acknowledgements

We thank the imaging platform of the Institut de Biologie Paris-Seine (IBPS), which is supported by CNRS, Sorbonne Université and the Conseil Régional of Ile de France. We also acknowledge Audrey Geeverding and Michaël Trichet from the IBPS electron microscopy core facility, and the IBPS aquatic platform for assistance and fish care. This research was supported by fundings from the French Muscular Dystrophy Association (AFM-Téléthon grant number 23545), the National Natural Science Foundation of China (grant number 32070813), and the annual supports from the Centre National de la Recherche Scientifique (CNRS) and the Sorbonne Université.

References

1. Glisovic T, Bachorik JL, Yong J, Dreyfuss G. RNA-binding proteins and post-transcriptional gene regulation. *FEBS Lett*. 2008; *582*:1977-1986. doi: 10.1016/j.febslet.2008.03.004.
2. Gebauer F, Schwarzl T, Valcárcel J, Hentze MW. RNA-binding proteins in human genetic disease. *Nat Rev Genet*. 2021; *22*:185-198. doi: 10.1038/s41576-020-00302-y.
3. Shi DL, Grifone R. RNA-binding proteins in the post-transcriptional control of skeletal muscle development, regeneration and disease. *Front Cell Dev Biol*. 2021; *9*:738978. doi: 10.3389/fcell.2021.738978.
4. Ladd AN. New insights into the role of RNA-binding proteins in the regulation of heart development. *Int Rev Cell Mol Biol*. 2016; *324*:125–85. doi: 10.1016/bs.ircmb.2015.12.009.
5. Shi, DL. RNA-binding proteins as critical post-transcriptional regulators of cardiac regeneration*. Int J Mol Sci.* 2023; *24*:12004. doi: 10.3390/ijms241512004.
6. Montañés-Agudo P, Pinto YM, Creemers EE. Splicing factors in the heart: Uncovering shared and unique targets. *J Mol Cell Cardiol*. 2023; *179*:72–79. doi: 10.1016/j.yjmcc.2023.04.003.
7. Fetka I, Radeghieri, A, Bouwmeester, T. Expression of the RNA recognition motif-containing protein SEB-4 during Xenopus embryonic development. *Mech Dev*. 2000; *94*:283–286. doi: 10.1016/s0925-4773(00)00284-7.
8. Grifone R, Xie X, Bourgeois A, Saquet A, Duprez D, Shi DL. The RNA-binding protein Rbm24 is transiently expressed in myoblasts and is required for myogenic differentiation during vertebrate development. *Mech Dev*. 2014; *134*:1–15. doi: 10.1016/j.mod.2014.08.003.
9. Miller RA, Christoforou N, Pevsner J, McCallion AS, Gearhart JD. Efficient array-based identification of novel cardiac genes through differentiation of mouse ESCs. *PLoS ONE.* 2008; *3*:e2176. doi: 10.1371/journal.pone.0002176.
10. Poon KL, Tan KT, Wei YY, Ng CP, Colman A, Korzh V, Xu XQ. RNA-binding protein RBM24 is required for sarcomere assembly and heart contractility. *Cardiovasc Res*. 2012; *94*:418–427. doi: 10.1093/cvr/cvs095.
11. Grifone R, Saquet A, Desgres M, Sangiorgi C, Gargano C, Li Z, Coletti D, Shi DL. Rbm24 displays dynamic functions required for myogenic differentiation during muscle regeneration. *Sci Rep.* 2021; *11*:9423. doi: 10.1038/s41598-021-88563-3.
12. Xu XQ, Soo SY, Sun W, Zweigerdt, R. Global expression profile of highly enriched cardiomyocytes derived from human embryonic stem cells. *Stem Cells*. 2009; *27*:2163–2174.doi: 10.1002/stem.166. PMID: 19658189.
13. Jin D, Hidaka K, Shirai M, Morisaki T. RNA-binding motif protein 24 regulates myogenin expression and promotes myogenic differentiation. *Genes Cells.* 2010; *15*:1158–1167. doi: 10.1111/j.1365-2443.2010.01446.x.
14. Liu J, Kong X, Zhang M, Yang X, Xu XQ. RNA binding protein 24 deletion disrupts global alternative splicing and causes dilated cardiomyopathy. *Protein Cell.* 2019; *10*:405–416. doi: 10.1007/s13238-018-0578-8.
15. Grifone R, Shao M, Saquet A, Shi DL. RNA-binding protein Rbm24 as a multifaceted post-transcriptional regulator of embryonic lineage differentiation and cellular homeostasis*. Cells.* 2020; *9*:1891. doi: 10.3390/cells9081891.
16. Zhang T, Lin Y, Liu J, Zhang ZG, Fu W, Guo LY, Pan L, Kong X, Zhang MK, Lu YH. Rbm24 regulates alternative splicing switch in embryonic stem cell cardiac lineage differentiation. *Stem Cells.* 2016; *34*:1776–1789. doi: 10.1002/stem.2366.

17. Yang J, Hung LH, Licht T, Kostin S, Looso M, Khrameeva EE, Bindereif A, Schneider A, Braun T. RBM24 Is a major regulator of muscle-specific alternative splicing. *Dev Cell.* 2014; *31*:87–99. doi: 10.1016/j.devcel.2014.08.025.
18. Zhang M, Zhang Y, Xu E, Mohibi S, De Anda DM, Jiang Y, Zhang J, Chen X. Rbm24, a target of p53, is necessary for proper expression of p53 and heart development. *Cell Death Differ.* 2018; *25*:1118–1130. doi: 10.1038/s41418-017-0029-8.
19. Maragh S, Miller RA, Bessling SL, McGaughey DM, Wessels MW, De Graaf B, Stone EA, Bertoli-Avella AM, Gearhart JD, Fisher S. Identification of RNA binding motif proteins essential for cardiovascular development. *BMC Dev. Biol*. 2011; *11*:62. doi: 10.1186/1471-213X-11-62.
20. Shao M, Lu T, Zhang C, Zhang YZ, Kong SH, Shi DL. Rbm24 controls poly(A) tail length and translation efficiency of crystallin mRNAs in the lens via cytoplasmic polyadenylation. *Proc Natl Acad Sci USA.* 2020; *117*:7245–7254. doi: 10.1073/pnas.1917922117.
21. Li HY, Bourdelas A, Carron C, Shi DL. The RNA-binding protein Seb4/RBM24 is a direct target of MyoD and is required for myogenesis during Xenopus early development. *Mech Dev.* 2010; *127*:281–291. doi: 10.1016/j.mod.2010.03.002.
22. Maragh, S.; Miller, R.A.; Bessling, S.L.; Wang, G.; Hook, P.W.; McCallion, A.S. Rbm24a and Rbm24b are required for normal somitogenesis. *PLoS ONE* 2014; *9*:e105460. doi: 10.1371/journal.pone.0105460.
23. Grunchec H, Deraze J, Dardalhon-Cuménal D, Ribeiro V, Coléno-Costes A, Dias K, Bloyer S, Mouchel-Vielh E, Peronnet F, Thomassin H. Single amino-acid mutation in a Drosophila melanogaster ribosomal protein: An insight in uL11 transcriptional activity. *PLoS One.* 2022; 17:e0273198. doi: 10.1371/journal.pone.0273198.
24. Wittwer, C.T.; Reed. G.H.; Gundry. C.N.; Vandersteen, J.G.; Pryor, R.J. High-resolution genotyping by amplicon melting analysis using LCGreen. *Clin Chem*. 2003, 49, 853–860. doi:10.1373/49.6.853.
25. Westerfield M. *The zebrafish book*. A guide for the laboratory use of zebrafish (Danio rerio). Univ. of Oregon Press: Eugene, USA (5th ed.); 2007.
26. O'Connor E, Phan V, Cordts I, Cairns G, Hettwer S, Cox D, Lochmüller H, Roos A. MYO9A deficiency in motor neurons is associated with reduced neuromuscular agrin secretion. *Hum Mol Genet.* 2018; *27*:1434–1446. doi: 10.1093/hmg/ddy054.
27. Ochi H, Westerfield M. Signaling networks that regulate muscle development: lessons from zebrafish. *Dev Growth Differ.* 2007; *49*: 1–11. doi: 10.1111/j.1440-169X.2007.00905.x.
28. Bakkers J. Zebrafish as a model to study cardiac development and human cardiac disease. *Cardiovasc Res.* 2011; *91*:279–288. doi: 10.1093/cvr/cvr098.
29. Sztal TE, Ruparelia AA, Williams C, Bryson-Richardson RJ. Using touch-evoked response and locomotion assays to assess muscle performance and function in zebrafish. *J Vis Exp.* 2016; *116*:54431. doi: 10.3791/54431.
30. Charvet B, Ruggiero F, Le Guellec D. The development of the myotendinous junction. A review. *Muscles Ligaments Tendons J*. 2012; *2*:53–63.
31. Carmignac V, Durbeej M. Cell-matrix interactions in muscle disease. *J Pathol.* 2012; *226*:200–218. doi: 10.1002/path.3020.
32. Long AM, Lee G, Demonbreun AR, McNally EM. Extracellular matrix contribution to disease progression and dysfunction in myopathy. *Am J Physiol Cell Physiol.* 2023; *325*:C1244–C1251. doi: 10.1152/ajpcell.00182.2023.
33. Charvet B, Guiraud A, Malbouyres M, Zwolanek D, Guillon E, Bretaud S, Monnot C, Schulze J, Bader HL, Allard B. Knockdown of col22a1 gene in zebrafish induces a muscular dystrophy by disruption of the myotendinous junction. *Development*. 2013; *140*:4602–4613. doi: 10.1242/dev.096024.

34. Hall TE, Bryson-Richardson RJ, Berger S, Jacoby AS, Cole, NJ, Hollway GE, Berger J, Currie PD. The zebrafish candyfloss mutant implicates extracellular matrix adhesion failure in laminin alpha2-deficient congenital muscular dystrophy. *Proc Natl Acad Sci USA.* 2007; *104*:7092–7097. doi: 10.1073/pnas.0700942104.
35. Jackson HE, Ingham PW. Control of muscle fibre-type diversity during embryonic development: the zebrafish paradigm. *Mech Dev.* 2013; *130*:447–457. doi: 10.1016/j.mod.2013.06.001.
36. Kemmler CL, Riemslagh FW, Moran HR, Mosimann C. From stripes to a beating heart: Early cardiac development in zebrafish. *J Cardiovasc Dev Dis.* 2021; *8*:17. doi: 10.3390/jcdd8020017.
37. Hinits Y, Osborn DP, Hughes SM. Differential requirements for myogenic regulatory factors distinguish medial and lateral somitic, cranial and fin muscle fibre populations. *Development*. 2009; *136*:403–414. doi: 10.1242/dev.028019.
38. Zhang M, Han Y, Liu J, Liu L, Zheng L, Chen Y, Xia R, Yao D, Cai X, Xu X. Rbm24 modulates adult skeletal muscle regeneration via regulation of alternative splicing. *Theranostics*. 2020; *10*:11159–11177. doi: 10.7150/thno.44389.
39 Lu SH, Lee KZ, Hsu PW, Su LY, Yeh YC, Pan CY, Tsai SY. Alternative splicing mediated by RNA-binding protein RBM24 facilitates cardiac myofibrillogenesis in a differentiation stage-specific manner. *Circ Res*. 2022; *130*:112–129. doi: 10.1161/CIRCRESAHA.121.320080
40. Jiang Y, Zhang M, Qian Y, Xu E, Zhang J, Chen X. Rbm24, an RNA-binding protein and a target of p53, regulates p21 expression via mRNA stability. *J Biol Chem*. 2014; *289*:3164–3175. doi: 10.1074/jbc.M113.524413.
41. Xu E, Zhang J, Zhang M, Jiang Y, Cho SJ, Chen X. RNA-binding protein RBM24 regulates p63 expression via mRNA stability. *Mol Cancer Res.* 2014; 12:359–369. doi: 10.1158/1541-7786.MCR-13-0526.

Legends to figures

Figure 1. Spatio-temporal expression of *rbm24a* transcripts during zebrafish development. (A-P) Lateral views, with anterior to the left, showing rbm24a expression in the developing somites from 8- to 24-somite stages (A-H) and progressively restricted to most caudal somites from 22 hpf to 31 hpf (I-P). (M'-O') Higher magnifications of the anterior region. (Q, R) Dorsal views, with anterior to the top, of the embryo at 10-somite stage shown in B, at the level of the anterior and posterior re-gions, respectively. (Q', R') Transverse sections at the levels indicated in Q and R, respectively. Note that rbm24a is expressed in the entire somite and in adaxial cells of the presomitic mesoderm. (S) Dorsal view, with anterior to the top, of the embryo at 22-somite stage shown in G, focused on the posterior region. (S'-S''') Transverse sections at the level indicated in S. (T) Dorsal view, with anterior to the top, of the embryo at 24 hpf shown in K, focused on the most posterior region. (T', T'') Transverse sections at the level indicated in T. (U-X) Dorsal views, with anterior to the right, of embryos presented in B-G, at the level of the heart area. The expression of rbm24a is also present in the developing heart (white arrows), otic placode (arrowheads), and lens (asterisks). So, somite; nt, neural tube; n, notochord; ad, adaxial cells; fmp, fast muscle progenitors; upm, unsegmented presomitic mesoderm. Scale bars: 100 μm.

Figure 2 . Spatio-temporal expression of *rbm24b* transcripts during zebrafish development. (A-K) Lateral views, with anterior to the left, of whole-mount embryos from 10-somite stage to 24 hpf, showing *rbm24b* expression in the developing somites. (A'-I') Dorsal views, with anterior to the top, of embryos shown in A-I, focused on the developing somites. (K) Weak *rbm24b* hybridization signal (outlined by dashed rectangle) can be observed in the heart area with prolonged incubation period for chromogenic reaction. (L) Transverse section of the embryo at 20-somite stage shown in F, at the level of somite (white arrow). (M) Transverse section of the embryo at 23 hpf shown in J, at the level of the somite (white arrow). So, somite; nt, neural tube; n, notochord. Scale bars: (A-K) 100 μm; (A'-I', L, M) 50 μm.

Figure 3. CRISPR/Cas9-mediated genome editing of *rbm24b* locus. (A) The genomic organization of *rbm24a* locus. The guide RNA targeting sequence in the first exon (E1) is underlined, and the PAM sequence is shown in blue. (B) Deletion of 8 nucleotides and insertion of 15 nucleotides (red) in the targeted region. (C) Schema of

Rbm24b protein domains and alignment of amino acids between wild-type and mutated Rbm24b proteins.The triangles indicate the position where amino acid change occurs or the last amino acid in the mutated Rbm24b protein.

Figure 4. Phenotype of *rbm24b* mutants at different stages. No morphological defects can be observed from blastula to 72 hpf.

Figure 5. Phenotypes of *rbm24a* and *rbm24b* mutants during early development. (A, D, G, J, M) Lateral views of wild-type embryos at indicated stages. (B, E, H, K, N) Lateral views of homozygous *rbm24a* single mutants show heart edema (arrows) at indicated stages. (C, F, I, L, O) Lateral views of double homozygous *rbm24a* and *rbm24b* mutants show an exacerbated heart edema (arrows) at different stages. At each developmental stage, 15 to 20 embryos per genotype were analyzed. Scale bars: 250 µm.

Figure 6. Disrupted integrity and function of skeletal muscles in *rbm24a* and *rbm24b* mutants. (A-C") Lateral views, anterior to the left, showing the muscle tissue. Scale bar: 250 µm. (D) Graph representing the average normalized area of skeletal muscle pixel intensities (mean grey values) shows the reduction of trunk muscle tissue in single and double mutants. At each developmental stage, 15 to 20 embryos per genotype were analyzed. (E-F") Lateral views comparing myofiber organization in *rbm24a* single mutants and *rbm24a*$^{-/-}$*;rbm24b*$^{-/-}$ double mutants. Scale bars: 25 µm. (G, G') Representative TEM images of skeletal muscle sections at 3 dpf show that the dark A-band and the light I-band patterning is severely disrupted by accumulation of disordered sarcoplasmic reticulum (black arrow) in double mutants (*n* = 4). Scale bars: 1 µm. (H) Graph comparing the velocity of *rbm24a* single mutants and *rbm24a*$^{-/-}$*;rbm24b*$^{-/-}$ double mutants at 2, 3 and 4 dpf. Average velocity with standard error were plotted and significant deviation was determined using the student's t-test. At each developmental stage, 15 to 20 embryos per genotype were analyzed.

Figure 7. Disrupted integrity and function of cardiac muscles in *rbm24a* and *rbm24b* mutants. (A-D') Immunofluorescence staining of ventricle and atria in wild-type embryos and *rbm24a*$^{-/-}$*;rbm24b*$^{-/-}$ double mutants. At each developmental stage, 15 to 20 embryos per genotype were analyzed. Scale bars: 5 µm. (E, F) Graphs measuring the ventricle and atrium size at 3 dpf and 4 dpf, respectively. (G, G') TEM images of heart sections. Wild-type embryos show highly organized sarcomeres with thin and thick

myofilaments in well-aligned bundles and discernible dark A-band and light I-bands, while double mutant embryos display a complete disorganization of sarcomeric unit. At each developmental stage, 15 to 20 embryos per genotype were analyzed. Scale bars: 500 nm. (H) Graph comparing heart rate of *rbm24a* single mutants and *rbm24a*$^{-/-}$*;rbm24b*$^{-/-}$ double mutants at 2, 3 and 4 dpf. Average heart rates with standard error were plotted and significant deviation was determined using the student's t-test. At each developmental stage, 15 to 20 embryos per genotype were analyzed.

Figure 8. Loss of *rbm24a* and *rbm24b* affects fast and slow muscle integrity. (A-D) Wild-type embryos at 2 dpf and 3 dpf stained with fast muscle (F310) and slow muscle (F59) antibodies. (A'-D') Reduced and disorganized fast and slow muscle in *rbm24a* and *rbm24b* double mutant embryos (*n* = 4). Scale bars: 25 μm.

Figure 9. Formation of myotendinous junction in *rbm24a* and *rbm24b* mutants. (A-F) DAPI staining. (A'-F') Laminin immunofluorescence staining. (A"-F'') Phalloidin staining. Lateral view for all embryos, with anterior to the right. Scale bar: 50 μm. Notice that myofibers appear dispersed and disorganized in *rbm24a* and *rbm24b* mutant embryos, whereas the myotendinous junction of somite boundaries exhibit a pattern similar to wild-type embryos. At each developmental stage, 15 to 20 embryos per genotype were analyzed. Scale bars: 25 μm.

Figure 10. Formation of neuromuscular junctions in *rbm24a* and *rbm24b* mutants. (A, B) Alpha-bungarotoxin staining. (A', B') Phalloidin staining. Lateral view of wild-type and *rbm24a*$^{-/-}$;*rbm24b*$^{-/-}$ mutant embryos at 4 dpf. Notice that myofibers appear dispersed and disorganized in *rbm24a* and *rbm24b* mutant embryos, whereas neuromuscular jonctions are present and are arborized in a smilar pattern as those vizualized in the wild-type. Scale bars: 50 μm

Figure1

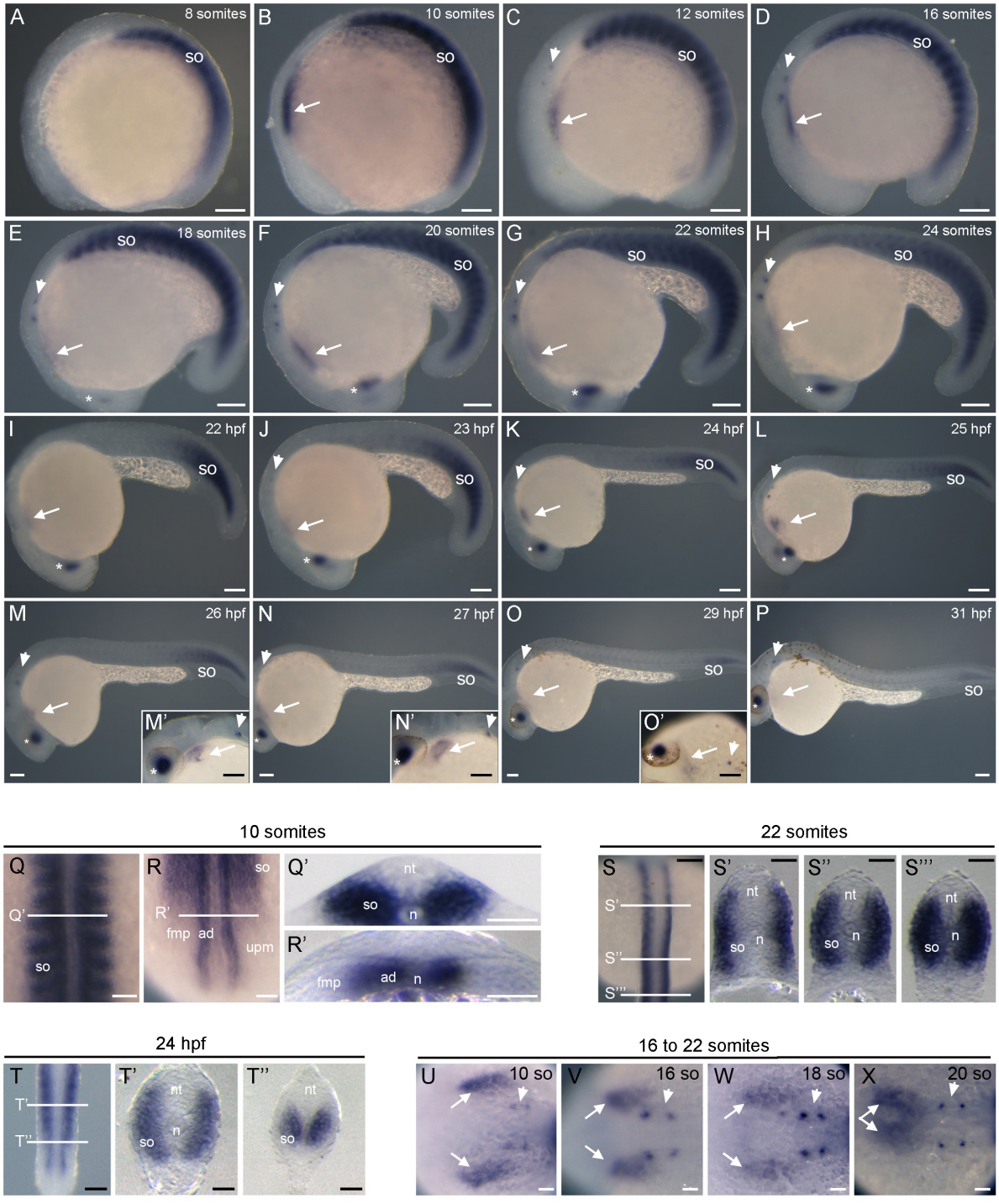
A
8 somites
so
B
10 somites
so
C
12 somites
so
D
16 somites
so
E
18 somites
so
F
20 somites
so
G
22 somites
so
H
24 somites
so
I
22 hpf
so
J
23 hpf
so
K
24 hpf
so
L
25 hpf
so
M
26 hpf
so
M'
N
27 hpf
so
N'
O
29 hpf
so
O'
P
31 hpf
so
10 somites
Q
Q'
so
R
so
R'
fmp ad
upm
Q'
nt
so
n
R'
fmp
ad
n
22 somites
S
S'
S''
S'''
S'
nt
so
n
S''
nt
so
n
S'''
nt
so
n
24 hpf
T
T'
T''
T'
nt
n
so
T''
nt
so
16 to 22 somites
U
10 so
V
16 so
W
18 so
X
20 so

Figure 2

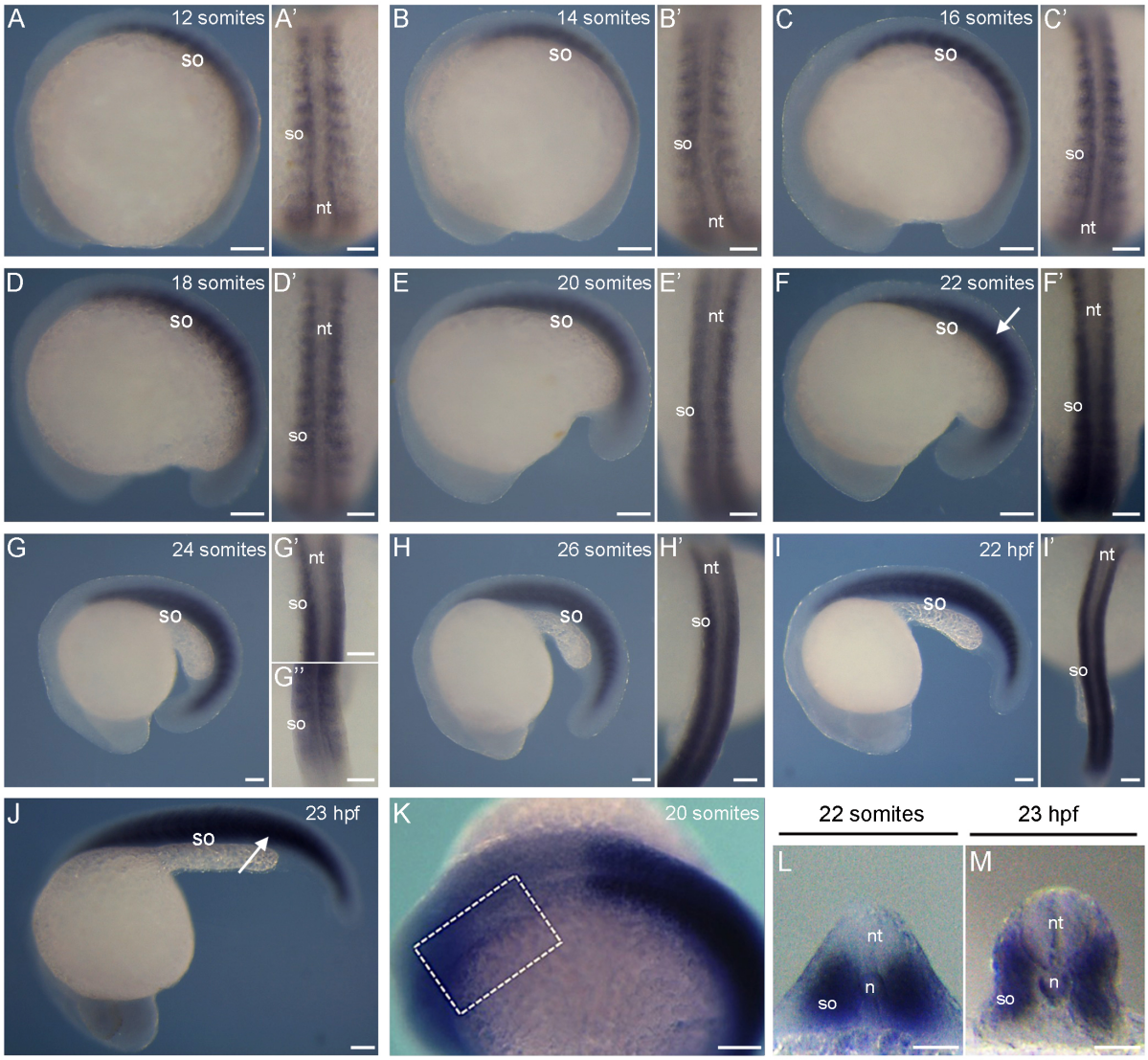
A
12 somites
so
A'
so
nt
B
14 somites
so
B'
so
nt
C
16 somites
so
C'
so
nt
D
18 somites
so
D'
nt
so
E
20 somites
so
E'
nt
so
F
22 somites
so
F'
nt
so
G
24 somites
so
G'
nt
so
G''
so
H
26 somites
so
H'
nt
so
I
22 hpf
so
I'
nt
so
J
23 hpf
so
K
20 somites
22 somites
23 hpf
L
nt
n
so
M
nt
n
so

Figure 3

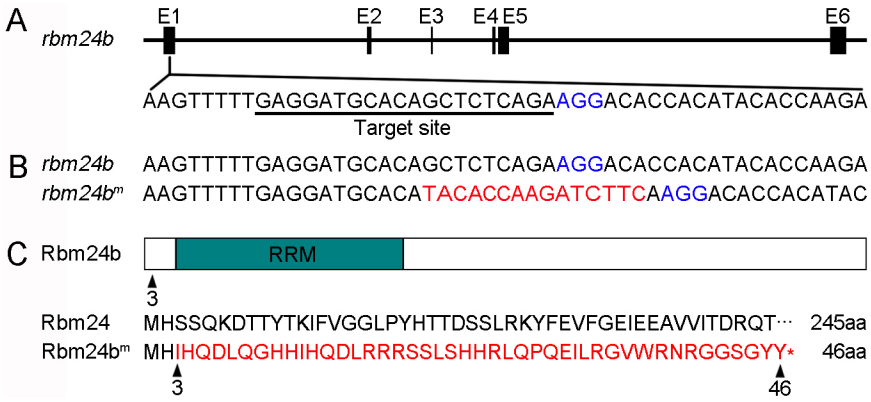

Figure 4

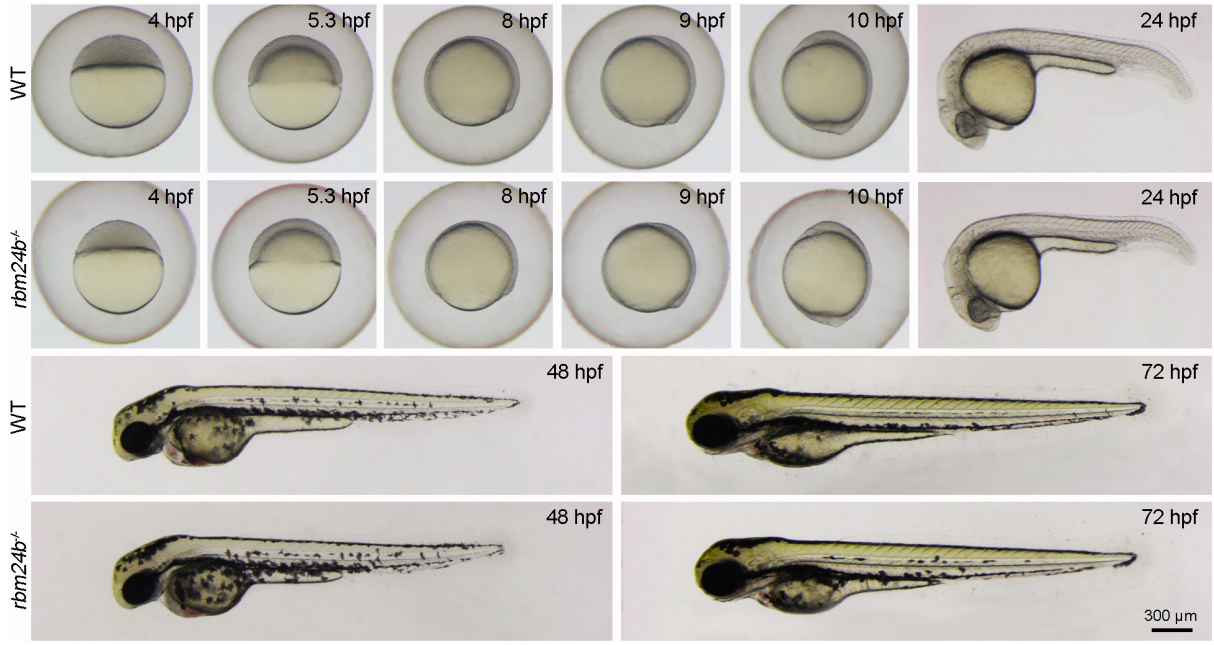

Figure 5

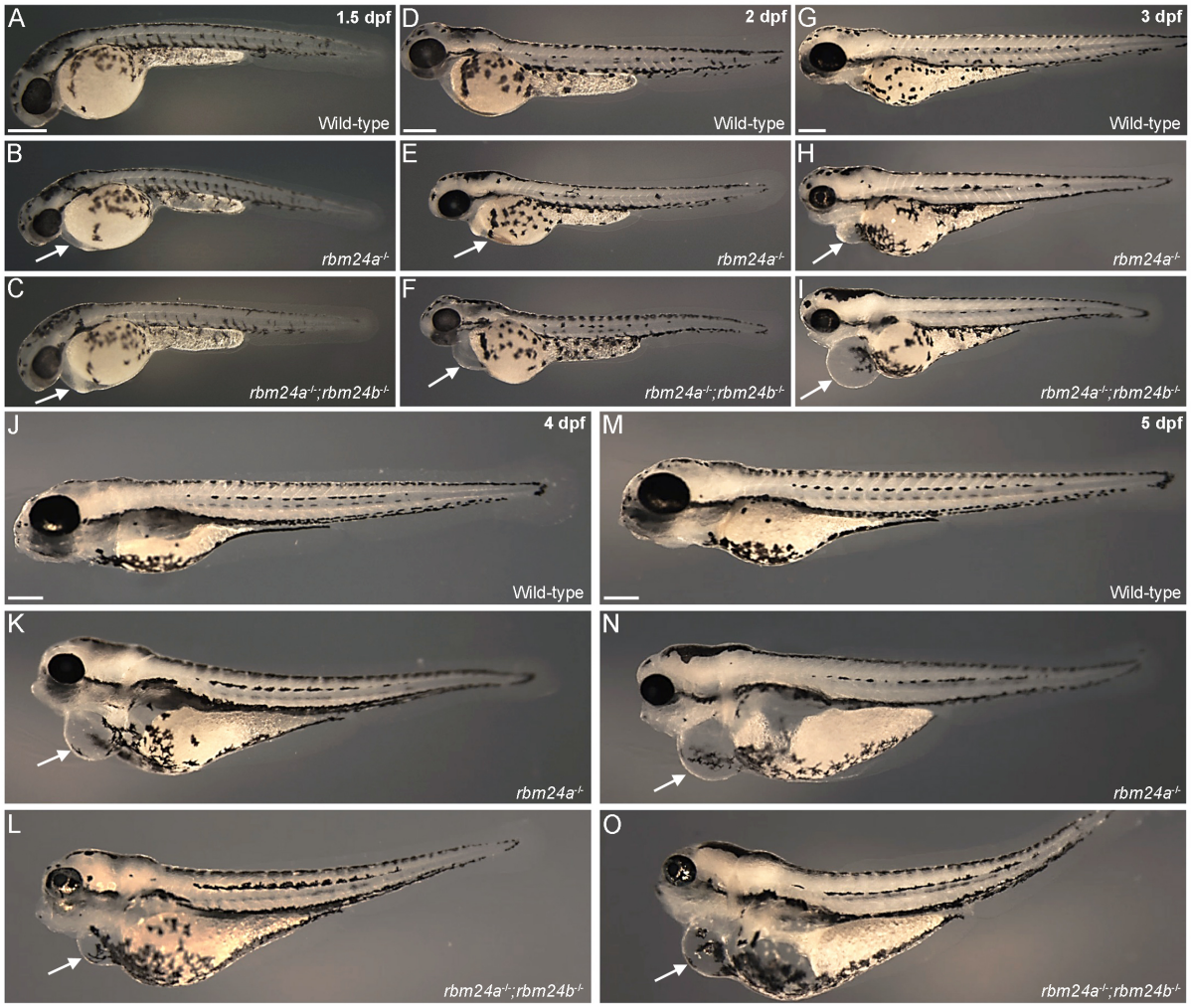
A
1.5 dpf
Wild-type
D
2 dpf
Wild-type
G
3 dpf
Wild-type
B
rbm24a-/-
E
rbm24a-/-
H
rbm24a-/-
C
rbm24a-/-;rbm24b-/-
F
rbm24a-/-;rbm24b-/-
I
rbm24a-/-;rbm24b-/-
J
4 dpf
Wild-type
M
5 dpf
Wild-type
K
rbm24a-/-
N
rbm24a-/-
L
rbm24a-/-;rbm24b-/-
O
rbm24a-/-;rbm24b-/-

Figure 6

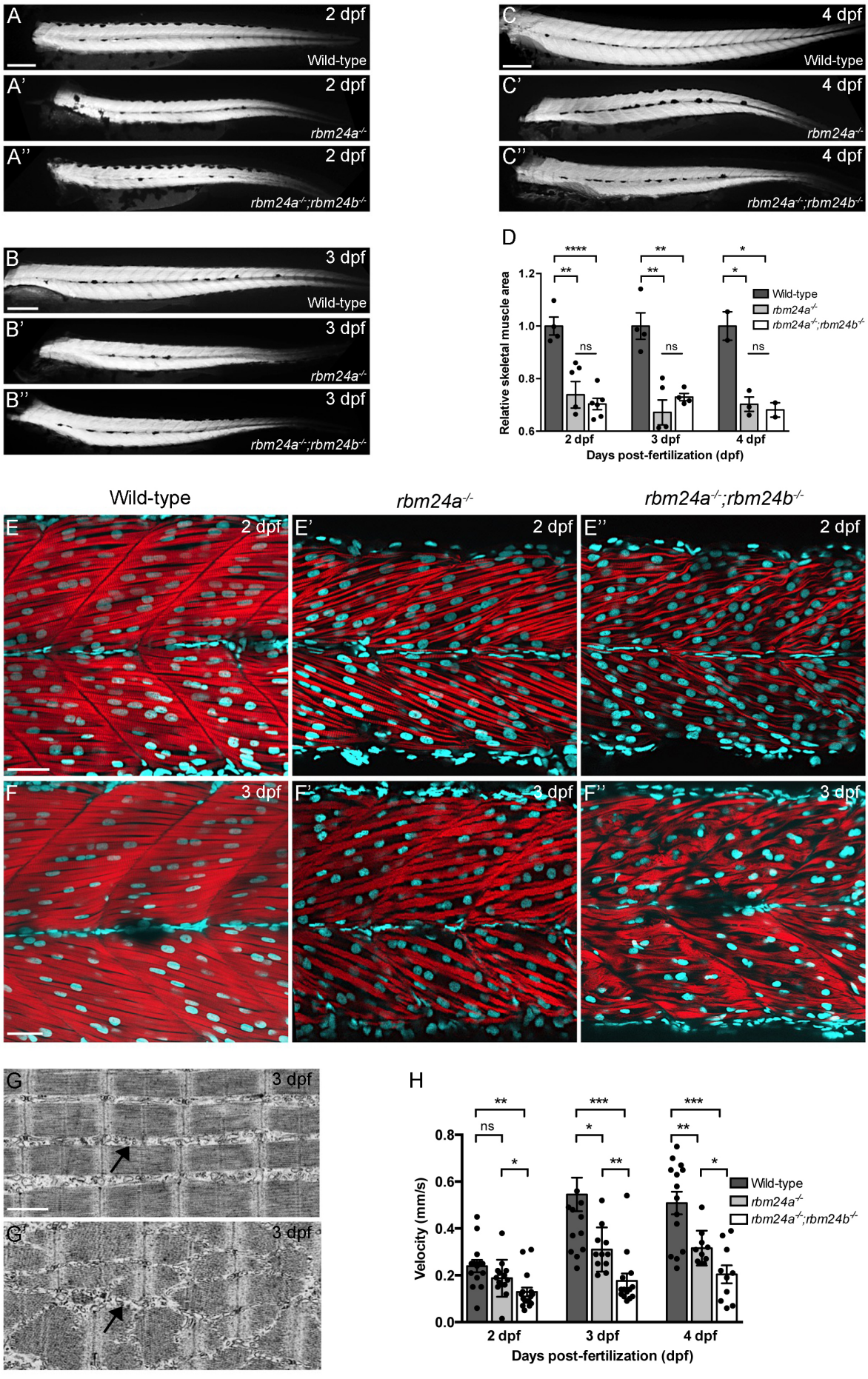
A
2 dpf
Wild-type
A'
2 dpf
rbm24a-/-
A''
2 dpf
rbm24a-/-;rbm24b-/-
B
3 dpf
Wild-type
B'
3 dpf
rbm24a-/-
B''
3 dpf
rbm24a-/-;rbm24b-/-
C
4 dpf
Wild-type
C'
4 dpf
rbm24a-/-
C''
4 dpf
rbm24a-/-;rbm24b-/-
D
Relative skeletal muscle area
1.2
1.0
0.8
0.6
****
**
**
**
*
*
ns
ns
ns
2 dpf
3 dpf
4 dpf
Days post-fertilization (dpf)
Wild-type
rbm24a-/-
rbm24a-/-;rbm24b-/-
Wild-type
rbm24a-/-
rbm24a-/-;rbm24b-/-
E
2 dpf
E'
2 dpf
E''
2 dpf
F
3 dpf
F'
3 dpf
F''
3 dpf
G
3 dpf
G'
3 dpf
H
Velocity (mm/s)
0.8
0.6
0.4
0.2
0.0
**
ns
*
***
*
**
***
**
*
2 dpf
3 dpf
4 dpf
Days post-fertilization (dpf)
Wild-type
rbm24a-/-
rbm24a-/-;rbm24b-/-

Figure 7

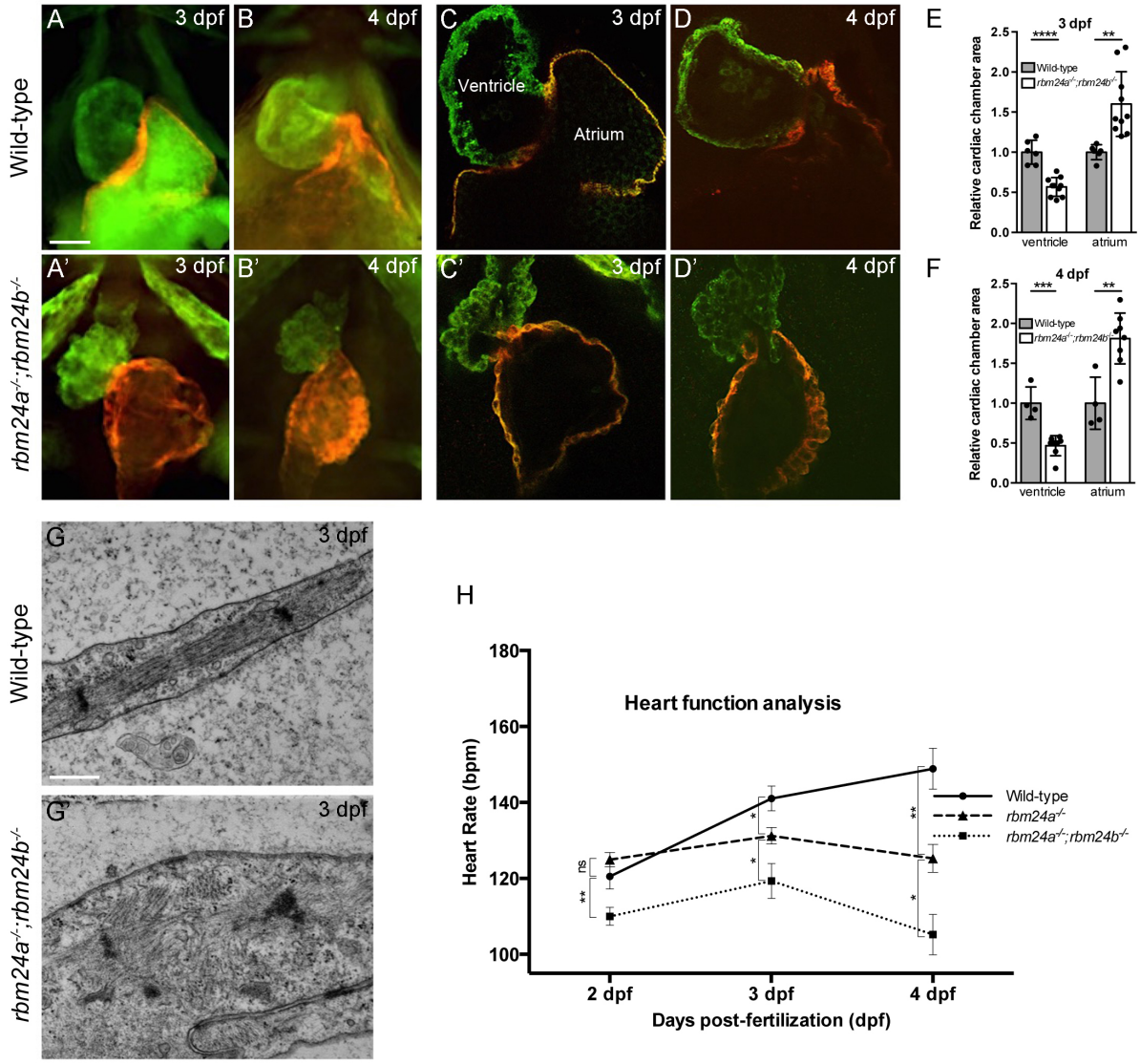
A
3 dpf
B
4 dpf
C
3 dpf
D
4 dpf
Ventricle
Atrium
Wild-type
A'
3 dpf
B'
4 dpf
C'
3 dpf
D'
4 dpf
rbm24a-/-;rbm24b-/-
E
3 dpf
****
**
Wild-type
rbm24a-/-;rbm24b-/-
Relative cardiac chamber area
2.5
2.0
1.5
1.0
0.5
0.0
ventricle
atrium
F
4 dpf
***
**
Wild-type
rbm24a-/-;rbm24b-/-
Relative cardiac chamber area
2.5
2.0
1.5
1.0
0.5
0.0
ventricle
atrium
G
3 dpf
Wild-type
G'
3 dpf
rbm24a-/-;rbm24b-/-
H
Heart function analysis
Heart Rate (bpm)
180
160
140
120
100
ns
**
*
*
**
*
Wild-type
rbm24a-/-
rbm24a-/-;rbm24b-/-
2 dpf
3 dpf
4 dpf
Days post-fertilization (dpf)

Figure 8

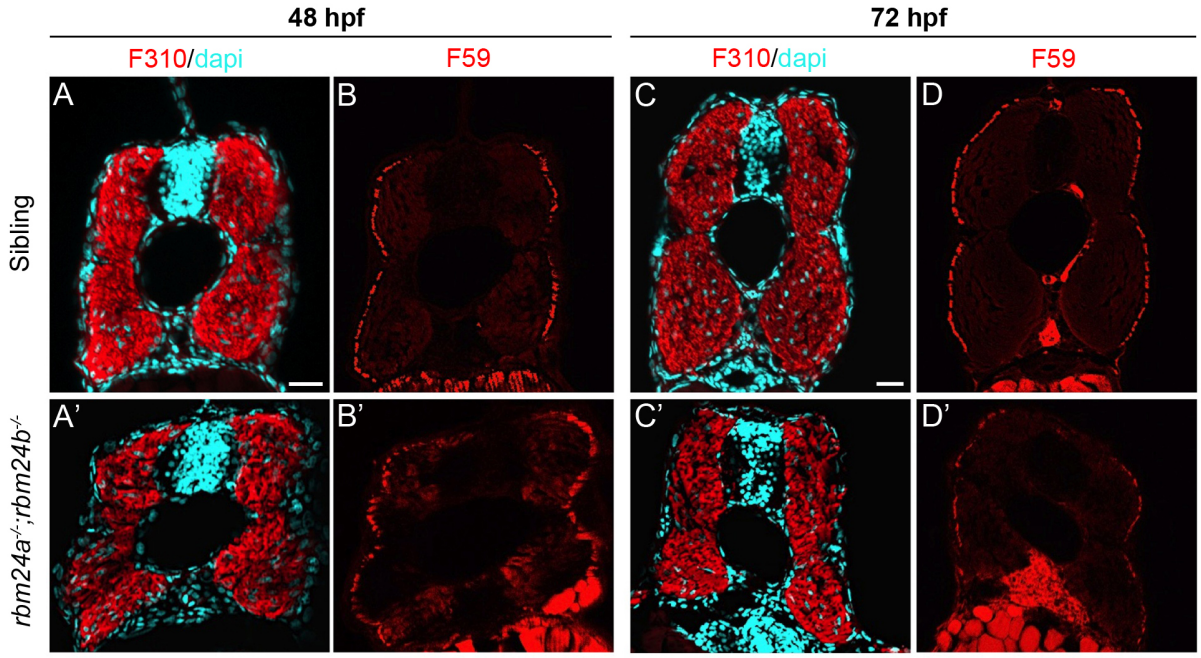
48 hpf
72 hpf
F310/dapi
F59
F310/dapi
F59
A
B
C
D
Sibling
A'
B'
C'
D'
rbm24a-/-;rbm24b-/-

Figure 9

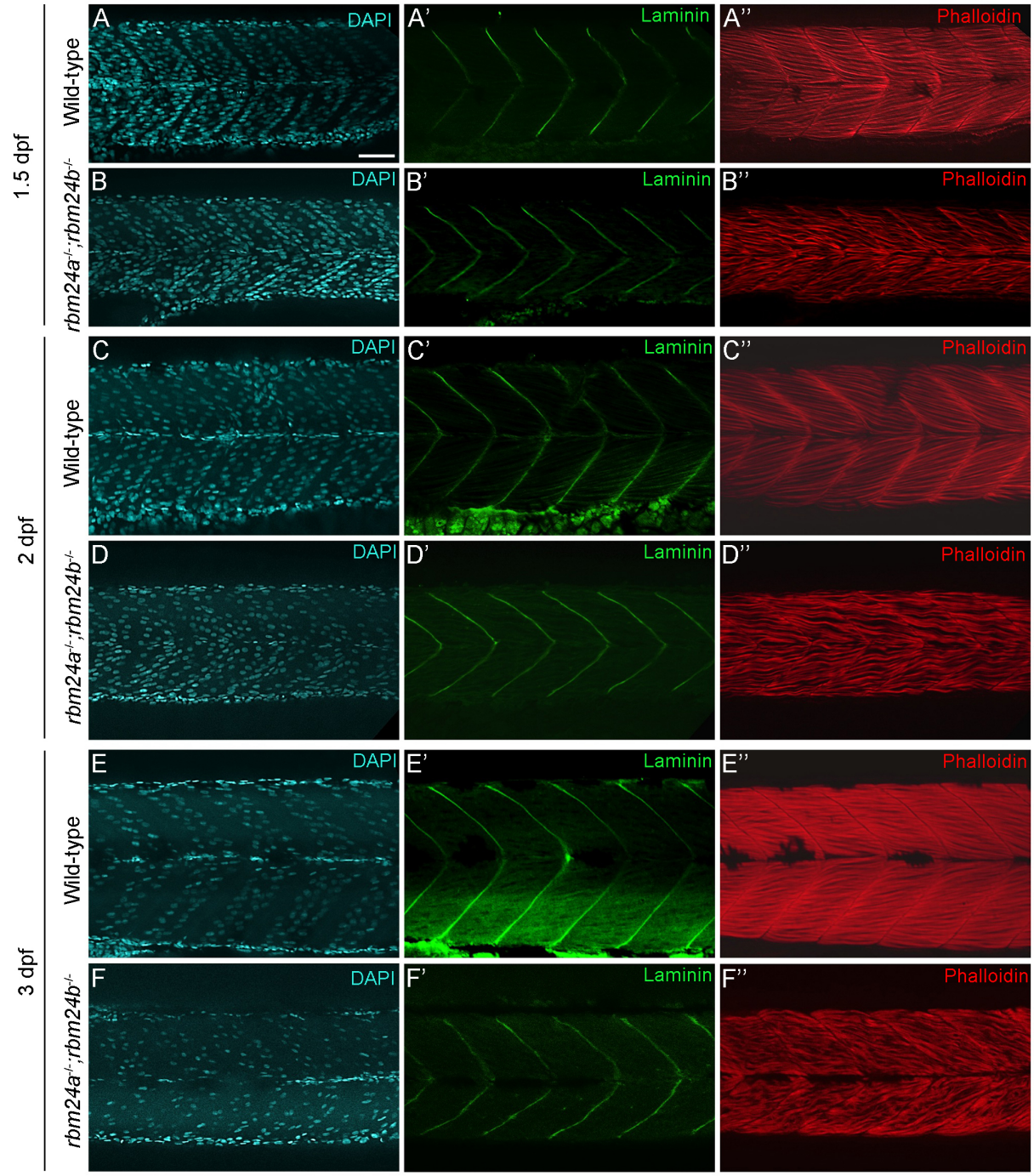
1.5 dpf
2 dpf
3 dpf
Wild-type
rbm24a-/-;rbm24b-/-
A
DAPI
A'
Laminin
A''
Phalloidin
B
B'
B''
C
C'
C''
D
D'
D''
E
E'
E''
F
F'
F''

Figure 10